Journal of Photochemistry and Photobiology A: Chemistry 217 (2011) 40–48

Contents lists available at ScienceDirect

Journal of Photochemistry and Photobiology A: Chemistry

journal homepage: www.elsevier.com/locate/jphotochem

Functional organogel based on a hydroxyl naphthanilide derivative and aggregation induced enhanced fluorescence emission

Manoj Kumar Nayak*

Department of Chemistry, Texas A&M University at Qatar, PO Box 23874, Doha, Qatar

ARTICLE INFO

Article history:
Received 17 June 2010
Received in revised form 29 July 2010
Accepted 21 September 2010
Available online 16 November 2010

Keywords:
Naphthanilide self-assembly
J-aggregation
Gelation-induced enhanced fluorescence emission (GIEFE)
Excited-state intramolecular proton transfer (ESIPT)
Twisted intramolecular charge transfer (TICT)

ABSTRACT

A new class of low molecular weight organogelator (LMOG) of hydroxyl naphthanilide moiety was suitably designed and synthesized and it forms gels through noncovalent interactions in hydrocarbon solvents. Self-assembly structure, hydrogen bonding interaction, and photophysical properties of organogelator 3-hydroxy-naphthalene-2-carboxylic acid (2-heptylcarbamoyl-phenyl)-amide (**2**) have been investigated by field emission scanning electron microscope (FE-SEM), FT-IR, UV–vis absorption and photoluminescence combined with theoretical studies by hybrid density-functional theory (DFT) B3LYP and semi-empirical calculations AM1 with CI methods. It was found that gelation is completely thermoreversible, and it occurs due to the aggregation of the organogelator resulting in the formation of a fibrous network due to the π–π stacking interaction complemented by the presence of both inter- and intra-molecular hydrogen bonding. The self-assembled fibrillar networks in the gels were distinctly evidenced by SEM observations. FT-IR studies confirm that the common driving force for aggregation in the organogels and microsegregation in the mesophase is the occurrence of a tight intermolecular hydrogen bonded network that does not persist in diluted solution. Gelator **2** is very weakly fluorescent in solution, but its intensity is increased by almost 30–32 times in their respective gelled state depending on the nature of the gelling solvents. The aggregation induced emission enhancement is ascribed to the formation of *J*-aggregation and inhibition of intramolecular rotation in the gel state.

1. Introduction

The search for efficient low molecular weight organic gelators with possible structure–activity correlation is on rise because of their diverse applications as supramolecular soft materials [1–6]. Organogels are usually assembled through self-aggregation of the small gelator molecules to form entangled supramolecular fibrillar networks via a combination of noncovalent interactions such as hydrogen bonding, π–π stacking, electrostatic forces, donor–acceptor interactions, metal coordination, solvophobic forces, and van der Waals interactions. The physical organogel is responsive to external stimuli such as thermo- [2], photo- [3], chemo- [4], metal- [5], proton- [6], and mechano- [1], by which the aggregate structure is stabilized or destabilized. In the stabilization process, the organogel structure is changed to a more ordered aggregation mode. On the other hand, in the destabilization process, the aggregate is dissociated to reversibly form a fluid liquid, indicating the gel-to-sol phase transition. The reversible systems can be potentially applied to drug delivery systems [7] and supramolecular switch system with memory function [8]. Moreover, some organogels displayed unique liquid crystalline properties, which are potential candidates for developing optical electronics [9]. Recently, there has been increasing interest in the development of functional organogels with π-conjugated moieties because of their potential applications involving nanomaterials such as, sensors [10], molecular electronics [11], enhanced charge transport [12], and light harvesting [13].

As an attempt to obtain a new functional organogelator with potential photonic applications in this work, the photoactive organogelator containing peripheral alkyl amide for gelation and 3-hydroxy-2-naphthanilide for fluorescence emission has been suitably designed and synthesized as shown in Fig. 1. In order to realize a rather simple but very efficient organogelator structure, long alkyl chains with an amide group, which are widely known for its typical gelation power, were selected and attached to the 3-hydroxy-2-naphthanilide part with unusual fluorescence. Fluorescence emission from 3-hydroxy-2-naphthanilide [14], and its resemblance 3-hydroxy-2-naphthoic acid [15], and *N*-(3-hydroxy-2-naphthamido)-*N*′-phenylthiourea [16] has been widely investigated and it was concluded that the emission originates from the excited-state intramolecular proton transfer (ESIPT) phenomenon. Hydroxyl naphthanilide derivatives have also been the subject of extensive investigations in medicinal chemistry, due to their ability to serve as potential cestodicidal agents [17]

* Tel.: +974 4423 0380; fax: +974 4423 0060.
E-mail addresses: manoj.nayak@qatar.tamu.edu, manoj@ipc.iisc.ernet.in

1010-6030/$ – see front matter © 2010 Elsevier B.V. All rights reserved.
doi:10.1016/j.jphotochem.2010.09.014

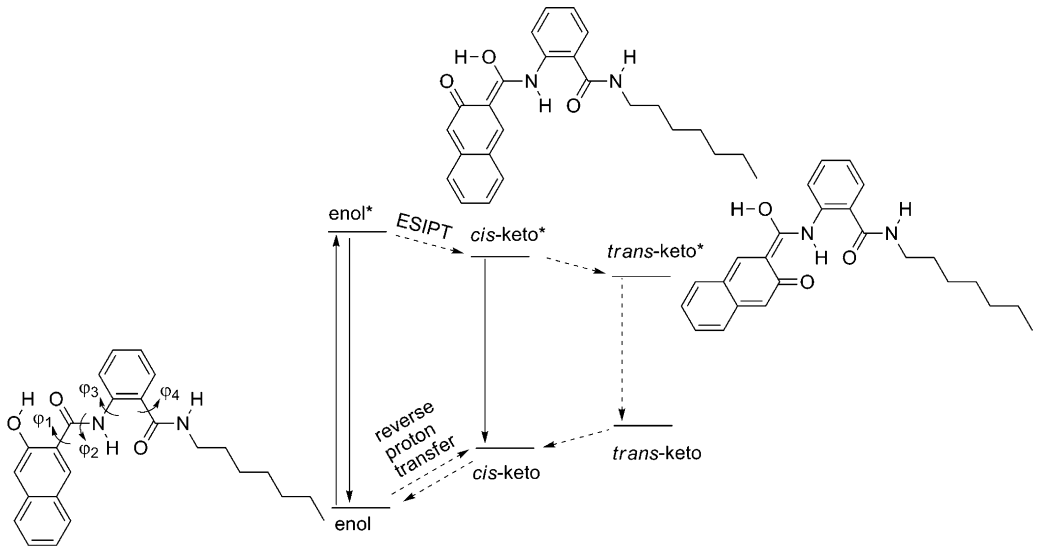

Fig. 1. The photochemical process leading to the formation of the *trans*-keto form from the enol form of naphthanilide gelator **2**. The solid arrows indicate the absorption phenomena or emission relaxation and the dotted arrows represent non-radiative relaxation.

and histochemical substrate for phosphatase [18]. However, the self-assembly behavior and related properties of naphthanilide derivatives remain unexplored in the field of functional gels and supramolecular organic soft materials. Target molecule of naphthanilide gelator **2** (Scheme 1) was designed to be capable of intermolecular as well as intramolecular hydrogen bonding. As a reference compound, 3-methoxy-2-naphthanilide derivative **3** was synthesized to investigate the specific role of ESIPT active 3-hydroxy-2-naphthanilide in **2** on the gelation properties. FE-SEM and FT-IR analyses were performed to probe the structure of gels, and also measured UV–vis absorption and photoluminescence (PL) with specific focus on the spectroscopic difference between solution and gel states. Whereas, the theoretical calculations were carried out to better understand the driving force for the aggregation mechanism and the ESIPT emission (Fig. 2).

2. Experimental

2.1. General

Proton and carbon magnetic resonance spectra (^{1}H NMR and ^{13}C NMR) were recorded on a Bruker Avance 500 (500 MHz) instrument using tetramethylsilane (0.03 (v/v)% TMS) in $CDCl_3$ as the internal standard (^{1}H NMR: TMS at 0.00 ppm, $CDCl_3$ at 7.24 ppm, and ^{13}C NMR: $CDCl_3$ at 77.23 ppm). Proton coupling patterns were

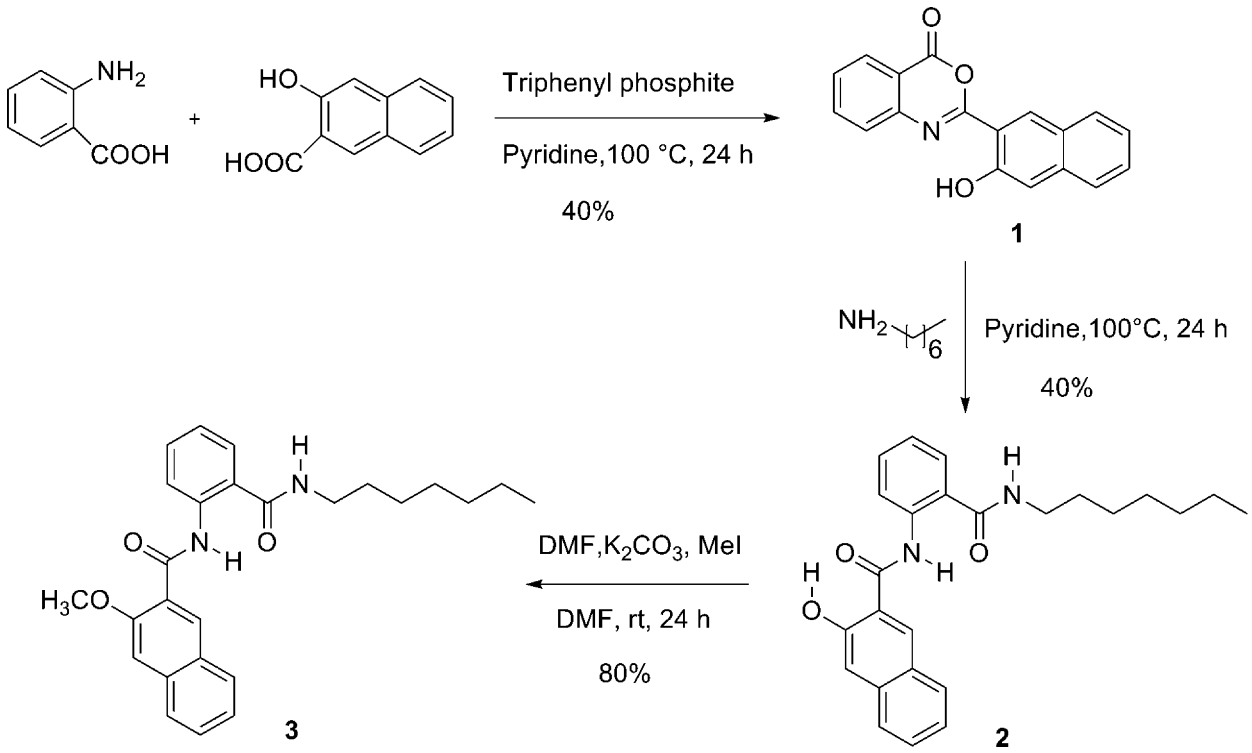

Scheme 1. Synthesis of naphthanilide-containing organogelator **2** and its non-ESIPT analogue **3**.

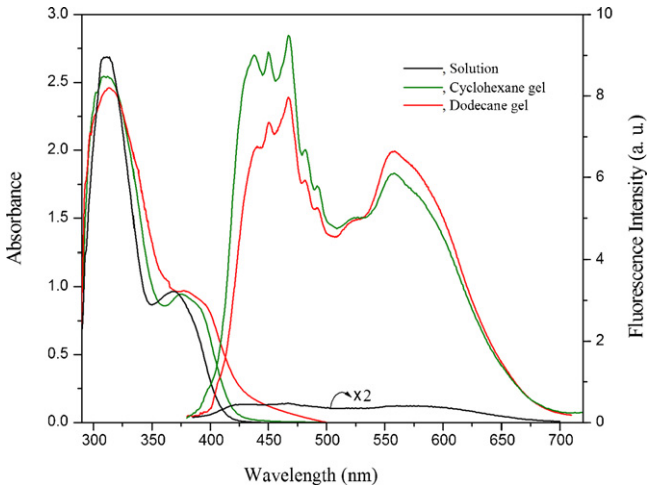

Fig. 2. UV–vis absorption at left and photoluminescence spectra at right of gelator **2** in solution (25 wt% of dioxane in cyclohexane), black; cyclohexane gel, green; and dodecane gel, red. (For interpretation of the references to color in this figure legend, the reader is referred to the web version of this article.)

described as singlet (s), doublet (d), triplet (t), quartet/quintet (q), multiplet (m) and broad (br). MS were recorded on a Kratos Concept H spectrometer (EI). Element contents of compounds were measured with EA1110 (CE Instrument, Italy). Differential scanning calorimetry (DSC) was performed on a PerkinElmer DSC-7 at heating rate of 20 °C min^{-1}. Infrared spectra were recorded using a PerkinElmer precisely Spectrum One FT-IR spectrometer in the range of 4000–500 cm^{-1}. UV–visible absorption and fluorescence spectra were recorded using Shimadzu UV-1650PC and Shimadzu RF-500 spectrofluorimeter, respectively, with emission and excitation slit width of 3 nm each. Field emission scanning electron microscopy (FE-SEM) images were obtained with a JSM-6330F (JEOL).

2.2. Synthesis of the organogelator [19]

2.2.1. 2-(3-Hydroxy-naphthalen-2-yl)-benzo[d][1,3]oxazin-4-one (**1**)

Anthranilic acid (3.0 g, 21.89 mmol) and 3-hydroxy 2-naphthoic acid (4.12 g, 21.89 mmol) were dissolved in pyridine (35 mL) and stirred for 30 min. Triphenyl phosphite (6.8 g, 21.89 mmol) was added to this solution and stirred at 100 °C for 4 h. The reaction mixture was poured into cold water and extracted with dichloromethane. The solution was dried with anhydrous magnesium sulfate. After removal of the solvent, the crude product was purified by column chromatography on silica gel with ethyl acetate/*n*-hexane (vol. ratio 1/3). The product was recrystallized from ethanol to give 2.53 g of pure product (yield 40%). m.p. 136 °C; ^{1}H NMR ($CDCl_3$, 500 MHz) δ = 12.05 (s, 1H), 8.74 (s, 1H), 7.86 (d, J = 8.20 Hz, 1H), 7.71 (d, J = 8.45 Hz, 1H), 7.53 (t, J = 7.50 Hz, 1H), 7.48 (t, J = 7.85 Hz, 2H), 7.35 (m, 3H), 7.26 ppm (t, J = 6.92 Hz, 2H); ^{13}C NMR ($CDCl_3$, 125 MHz) δ = 168.89, 156.79, 150.47, 138.59, 133.38, 129.93, 129.80, 129.62, 127.42, 126.73, 126.65, 124.42, 121.90, 113.96, 112.27 ppm; MS (EI) m/z 289.10 (M^+, 100.0), 261 (M^+, 18.9), 233 (M^+, 4.5), 217 (M^+, 2.6), 171 (M^+, 10.8), 142 (M^+, 13.4), 114 (M^+, 8.0), 92 (M^+, 1.6); Element analysis calcd (%) for $C_{18}H_{11}NO_3$: C 74.73, H 3.83, N 4.84 and O 16.59; found: C 74.76, H 3.87, N 4.80 and O 16.61.

2.2.2. 3-Hydroxy-naphthalene-2-carboxylic acid (2-heptylcarbamoyl-phenyl)-amide (**2**)

Compound **1** (1.0 g, 3.46 mmol) and *n*-heptylamine (1.98 g, 16.5 mmol) were dissolved in pyridine (32 mL). The solution was heated at 100 °C and refluxed under N_2 atmosphere for 24 h. The reaction mixture was poured into cold water and neutralized with 1 N HCl solution, after which the precipitate was collected by filtration. The crude product was purified by column chromatography on silica gel with ethyl acetate/*n*-hexane (vol. ratio 1/10). The product was recrystallized from ethanol to give 0.55 g of pure product (yield 40%). m.p. 147.7 °C; ^{1}H NMR ($CDCl_3$, 500 MHz) δ = 12.66 (s, 1H), 11.81 (s, 1H), 8.66 (d, J = 8.30 Hz, 1H), 8.36 (s, 1H), 7.92 (d, J = 8.26 Hz, 1H), 7.67 (d, J = 8.35 Hz, 1H), 7.52 (q, J = 7.17 Hz, 2H), 7.47 (t, J = 7.46 Hz, 1H), 7.31 (t, J = 7.47 Hz, 2H), 7.14 (t, J = 7.65 Hz, 1H), 6.33 (s, 1H), 3.48 (q, J = 7.0 Hz, 2H), 1.65 (q, J = 7.30 Hz, 2H), 1.42–1.30 (m, 8H), 0.85 ppm (t, J = 6.39 Hz, 3H); ^{13}C NMR ($CDCl_3$, 125 MHz) δ = 169.29, 169.11, 157.50, 139.22, 137.48, 132.85, 129.59, 128.88, 128.56, 127.36, 126.66, 126.29, 123.93, 123.82, 122.39, 121.49, 117.86, 112.56, 40.44, 31.93, 29.73, 29.15, 27.19, 22.78, 14.21 ppm; MS (EI) m/z 404.1 (M^+, 14.5), 289 (M^+, 100.0), 261 (M^+, 5.4), 233 (M^+, 1.5), 171 (M^+, 10.4), 142 (M^+, 9.2), 115 (M^+, 9.8), 92 (M^+, 1.8); HRMS calcd for $C_{25}H_{28}N_2O_3$: 404.50, found: 404.21; IR (KBr pellet, cm^{-1}) 3414.5 (ν_{OH}), 3309.5 (ν_{NH}), 1595.2 (ν_{CO}), 1530.8 (δ_{NH}); Element analysis calcd (%) for $C_{25}H_{28}N_2O_3$: C 74.23, H 6.98, N 6.93 and O 11.87; found: C 74.0, H 7.01, N 6.95 and O 11.75.

2.2.3. 3-Methoxy-naphthalene-2-carboxylic acid (2-heptylcarbamoyl-phenyl)-amide (**3**)

Compound **2** (0.3 g, 0.74 mmol) was dissolved in DMF (8 mL) at room temperature. K_2CO_3 (0.12 g, 0.86 mmol) and MeI (0.12 g, 0.82 mmol) were added to this solution. The reaction mixture was stirred under dark conditions for 24 h. This solution was poured to cold water and precipitate was collected by filtration. The crude product was purified by column chromatography on silica gel using eluent 1–2 (v/v)% of ethyl acetate in *n*-hexane to give 0.25 g of pure product (yield 80%). m.p. 156 ± 3 °C; ^{1}H NMR ($CDCl_3$, 500 MHz) δ = 11.75 (s, 1H), 8.73 (s, 1H), 8.69 (d, J = 8.36 Hz, 1H), 7.88 (d, J = 8.15 Hz, 1H), 7.73 (d, J = 8.25 Hz, 1H), 7.48 (q, J = 7.74 Hz, 2H), 7.42 (d, J = 7.65 Hz, 1H), 7.36 (t, J = 7.50 Hz, 1H), 7.23 (d, J = 5.67 Hz, 1H), 7.07 (t, J = 7.47 Hz, 1H), 6.14 (s, 1H), 4.16 (s, 3H), 3.42 (q, J = 6.70 Hz, 2H), 1.58 (q, J = 7.35 Hz, 2H), 1.36–1.25 (m, 8H), 0.82 ppm (t, J = 7.05 Hz, 3H); ^{13}C NMR ($CDCl_3$, 125 MHz) δ = 168.99, 164.36, 155.21, 138.50, 136.25, 134.10, 131.81, 129.40, 128.47, 126.73, 126.43, 125.12, 124.56, 124.04, 123.44, 123.43, 107.60, 55.93, 40.18, 31.93, 29.89, 29.19, 27.19, 22.77, 14.19 ppm; MS (EI) m/z 418.1 (M^+, 28.1), 304 (M^+, 32.5), 276 (M^+, 11.0), 234 (M^+, 20.5), 185 (M^+, 100.0), 170 (M^+, 3.0), 152 (M^+, 7.0), 127 (M^+, 14.5), 120 (M^+, 5.6), 114 (M^+, 3.4); HRMS calculated for $C_{26}H_{30}N_2O_3$: 418.53, found: 418.22; Elemental analysis calcd (%) for $C_{26}H_{30}N_2O_3$: C 74.61, H 7.22, N 6.69 and O 11.47; found: C 74.80, H 7.52, N 6.41 and O 10.85.

2.3. Preparation of gels and determination of gelation temperatures

Weighed amounts of organogelators were added to the solvent and heated until all organogelators were fully dissolved. The solution was then left as such, until it cooled down to room temperature. The inverted test tube method was used to examine the gel formation in different solvents and to determine critical gelation concentration (CGC). The ball dropping method was used to determine the sol–gel phase-transition temperature (T_{gel}).

2.4. UV–vis absorption and photoluminescence (PL)

To get proper absorbance, a UV-cell for opaque gel was made to give 1 mm path length, photoluminescence of opaque liquids and solids was carried in the same cuvette by front-face detection technique at an angle that minimizes reflected and scattered light. Photoluminescence quantum efficiencies (Φ_{PL}) for solutions were obtained using 9,10-diphenylanthracene as a reference [20]. On the

Table 1
Basic properties of organogels.

Compound	Shape	CGC	Solvent	Transparency	T_{gel} (°C)
2	Gel	0.25 wt%	Cyclohexane, dodecane	Translucent	74
				Opaque	81
3	Precipitate		Cyclohexane, dodecane		

other hand, Φ_{PL} of PMMA film doped with 10 wt% of organogelator **2** and **3** were measured using a 6-in. integrating sphere (Labsphere, 3P-GPS-060-SF) equipped with a 325-nm CW He–Cd laser (Omnichrome, Series 56) and a PMT detector (Hamamatsu, PD471) attached to a monochromator (Acton Research, Spectrapro-300i). The detailed analytical procedure to obtain solid-state Φ_{PL} has been described elsewhere [21].

2.5. Computational details

All molecular structures were fully optimized using the hybrid B3LYP functional method [22], in combination with 6-31G(d,p) Gaussian basis set. For each optimized structure a frequency analysis at the same level of theory was used to verify that it corresponds to a stationary point in the potential energy surface. As the use of diffuse functions is essential for accurate determination of the energetics, particularly for ion radicals and excited states [23], to perform a singlet-point calculation on the basis of B3LYP/6-31G(d,p) optimized structures. The excited-state properties were calculated with the time-dependent density functional theory (TD-DFT) [24] formalism, using the optimized ground state geometries. TD-DFT in combination with the B3LYP hybrid functional and the 6-31G(d,p) basis set has previously been shown to provide accurate energies for excited states within 0.2 eV (5 kcal mol^{-1}) [25]. All calculations were performed with the Gaussian 03 package of programs [26].

In addition to high level DFT calculations, semi-empirical methods offer an attractive alternative for studying potential energy surfaces in ground and excited states. Procedures such as the AM1 method [27] allow examination of potential energy surfaces without geometric assumptions. With inclusion of limited configuration interaction, especially through the single and pair double excitation (PECI) procedure [28], spectral properties of several conjugated organic systems have been shown to be reliably reproduced [29,30]. Therefore, the spectral properties of ESIPT gelator **2** have been simulated using AM1/PECI = 8 calculations in order to guide the synthetic efforts towards materials with enhanced performances and to help with the interpretation of the experimental data. The geometry dependent potential energies in the ground (S_0) and first excited (S_1) states were calculated by changing geometrical parameters of interest from the optimized geometry. In these calculations, all the geometrical parameters were optimized at each point.

3. Results and discussion

3.1. Synthesis and self-assembly structure of organogels

Ortho-substituted *N*-heptyl amide derivatives of 3-hydroxy-2-naphthanilide (**2**) and its non-ESIPT analogue (**3**) were synthesized according to our earlier reported literature procedure [19] and are depicted in Scheme 1. The cyclized intermediate 3-hydroxynaphthyl-benzoxazin-4-one (**1**) was prepared by dehydrocyclization reaction between 3-hydroxy 2-naphthoic acid and anthranilic acid using triphenyl phosphite in pyridine in 40% yield. Amidolysis reaction of **1** with *n*-heptylamine in pyridine led to the ESIPT gelator **2** in 40% yield. Subsequently, *O*-methylation reaction of **2** with equimolar amount of MeI and potassium carbonate in DMF led to the non-ESIPT analogue **3** in good yield of 80%. The molecular structures were fully characterized through Fourier transform infrared (FT-IR) spectroscopy, ^{1}H and ^{13}C NMR, MS-EI/HRMS spectral evidence and elemental analysis.

The gelation ability of organogelator **2** was tested in various organic solvents and it was able to induce gelation in non-polar solvents such as dodecane and cyclohexane with critical gelation concentrations (CGC) as low as 0.25 wt%, but not in polar solvents as summarized in Table 1. It is most likely that the intramolecular hydrogen bonding of 3-hydroxy-2-naphthanilide group in **2** is essential for the gelation behavior, since its methoxy derivative **3** without that structural element is not able to gel a solvent but form needle shape crystals (Fig. 3). This result implies that the intramolecular hydrogen bonding in 3-hydroxy-2-naphthanilide unit contributes to the planarization effect not only allowing ESIPT but also improving the favorable π-stacking for the gelation (*vide infra*).

In order to discern the nature of the microstructures that may be present in such gels with such varying gelation capacity and mechanical strength, the morphology of the xerogels obtained from **2** in cyclohexane and dodecane was examined by field emission scanning electron microscope (FE-SEM). The FE-SEM images (Fig. 4) show their nanoscale assembly in different organic solvents, and this indicates that compound **2** possesses the directional forces required for the unidirectional intermolecular interactions between the gelator molecules to form the fibrous nanoscale architecture [31]. Careful analysis revealed the flexible fibrillar aggregates obtained from cyclohexane gel are approximately 50–60 nm in width and ~2–5 μm in length. However, the dodecane gels obtained from **2** showed relatively thicker fibers of diameter ~1–2 μm and several micrometers (~15–25 μm) in length. In all the cases one can observe a network structure composed of fibrous aggregates. This means that the gel fibers present probably consist of hierarchical structures.

Considering the structure of the LMOG prepared in this work, and the well-known fact that hydrogen bonding interaction among the amide groups is one of the main driving forces for the self-assembly of organogelators in organic solvents. FT-IR is an important tool for investigating the different non-covalent interactions involved in gelation [32–36]. To obtain structural information about self-assembled material FT-IR was measured at three different states: solution (1 wt%) in chloroform, gel (1 wt%) in cyclohexane and solid powder. In solution state, four main characteristic peaks appeared at 3448.5, 3315.2, 2925.5, 2854.0, 1594.9, and 1529.0 cm^{-1} for O–H, amide N–H asymmetric stretching (ν_{OH}, ν_{NH}), antisymmetric (ν_{as}) and symmetric (ν_s) CH_2 stretching frequency bands, amide C=O ν_{CO} (amide I), and N–H bending δ_{NH} (amide II), respectively (representative spectra of **2**, Figs. 5 and S6, and Table S1). As far as gel (solid powder) material was concerned the N–H stretching, the amide I band and N–H bending peaks are shifted to 3310.2 (3309.5), 1594.0 (1595.2), and 1525.5 (1530.8) cm^{-1}, respectively. The red shifts of N–H stretching as well as the blue shift of N–H bending band indicate that intermolecular hydrogen bond formation occurs in the gel state and no band was observed above 3400 cm^{-1} in the gel state indicating the presence of hydrogen bonded NH in the supramolecular gel network.

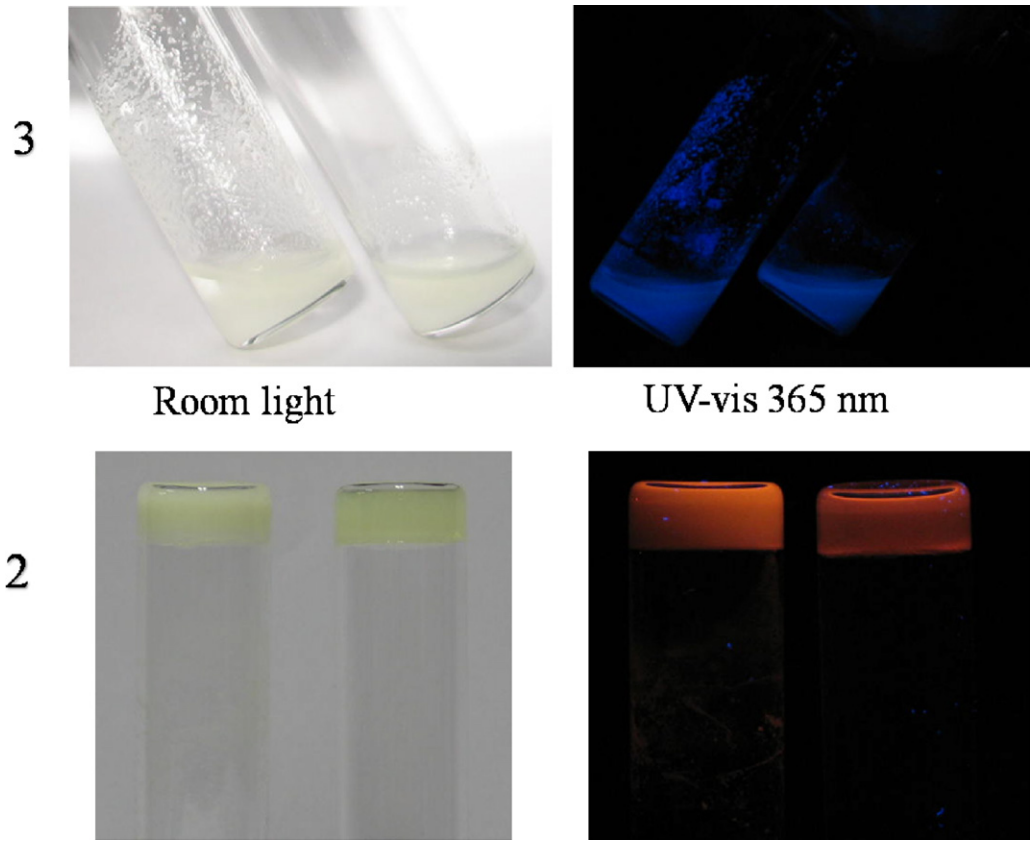

Fig. 3. Images 1 wt% of gelator **2** in dodecane and cyclohexane (bottom); 2 wt% of non-ESIPT analogue **3** is prepared in dodecane and cyclohexane (top) at room light and under UV light at 365 nm.

The O–H stretching frequency observed in solid state appeared at 3414.5 cm^{-1} (ν_{OH} 3448.5 cm^{-1} in solution phase) is also suggesting the presence of strong intramolecular hydrogen bonding association in that dried gel. Also, the shifting of antisymmetric (ν_{as}) and symmetric (ν_s) CH_2 stretching frequency bands was observed from 2929.5 and 2856.4 cm^{-1} in the solution phase to 2925.0 and 2853.8 cm^{-1} in the gel state, respectively. The decrease in fluidity of the hydrophobic chains due to the formation of aggregates via van der Waals interaction is evident from this particular shift in the CH_2 stretching frequency [33]. The facts indicate that the presence of intermolecular hydrogen bonding among the amide groups and intramolecular OH···O=C hydrogen bonding and van der Waals interaction plays an essential role in the self-aggregation of this gelator **2**.

3.2. Photo-physicochemical properties of naphthanilides and gelation-induced enhanced fluorescence emission

This class of gelator being chromophoric allows evaluation of their optical and photophysical properties on self-assembly. To study the spectroscopic properties of self-assembled aggregates, UV–vis absorption and photoluminescence spectra of compounds **2** and **3** were investigated in details in different solvents (shown in Figs. 2 and 6 and summarized data in Table 2). Absorption band maxima (λ^{ab}_{max}) for all the bands of compound **2** are blue shifted and ε_{max} decreases with increase in the solvent polarity and their protic nature of the solvents. Long wavelength (LW) tautomer emission observed in cyclohexane is independent of λ_{exc}, but in less polar aprotic solvents dual fluorescence is observed only at λ_{exc} > 350 nm.

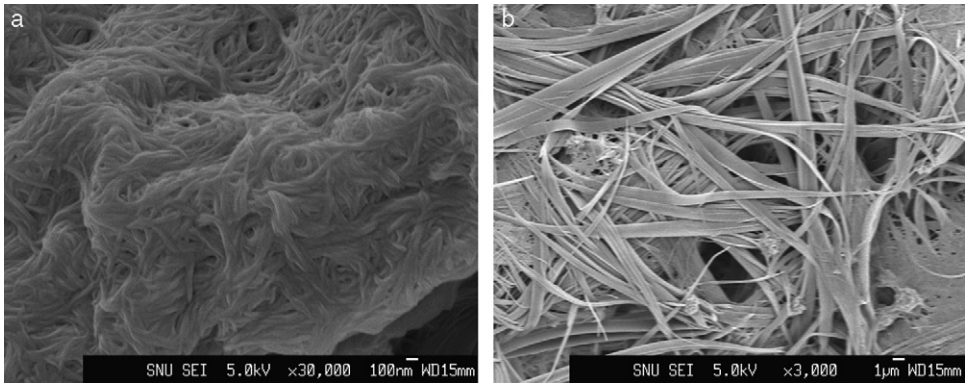

Fig. 4. Field emission scanning electron microscope images of xerogel **2** in (a) cyclohexane and (b) dodecane.

Table 2
Absorption band maxima (λ^{ab}_{max}, nm) and fluorescence band maximum (λ^{fl}_{max}, nm) and fluorescence quantum yield (Φ_{fl}) of **2** (concentration = 1×10^{-5} M, λ_{exc} = 370 nm) and **3** (concentration = 2×10^{-5} M, λ_{exc} = 300 nm) in different solvents.

Solvents	**2**		**3**	
	λ^{ab}_{max}, nm (log ε_{max})	λ^{fl}_{max}, nm (Φ_{fl})	λ^{ab}_{max}, nm (log ε_{max})	λ^{fl}_{max}, nm (Φ_{fl})
Cyclohexane	315, 375 (4.14), (3.51)	446, 574 (0.002)	296, 355	364, 380 (0.054)
Chloroform	314, 374 (4.14), (3.46)	432, 564 (0.0016)	300, 356 (4.30), (3.27)	389 (0.015)
Acetonitrile	312, 372 (4.13), (3.45)	415, 563 (0.002)	299, 356 (4.29), (3.23)	390 (0.012)
1-Propanol	307, 368 (4.13), (3.42)	425, 501 (0.042)	301, 356 (4.33), (3.26)	396 (0.029)
Methanol	303, 367 (4.14), (3.39)	427, 526 (0.023)	299, 355 (4.31), (3.24)	406 (0.021)
PMMA film (10 wt% of sample)	306, 366	393, 558 (0.021)	299, 352	386 (0.120)
Gelation study (0.5 wt% sample)				
Dodecane gel	313, 378	439, 450, 467, 558		
Cyclohexane gel	312, 375	438, 450, 467, 557		
Solution (25 wt% of dioxane in cyclohexane)	299, 352	428, 466, 572		

Underline is to distinguish two most intense peaks from the structured fluorescence bands obtained in the gel states.

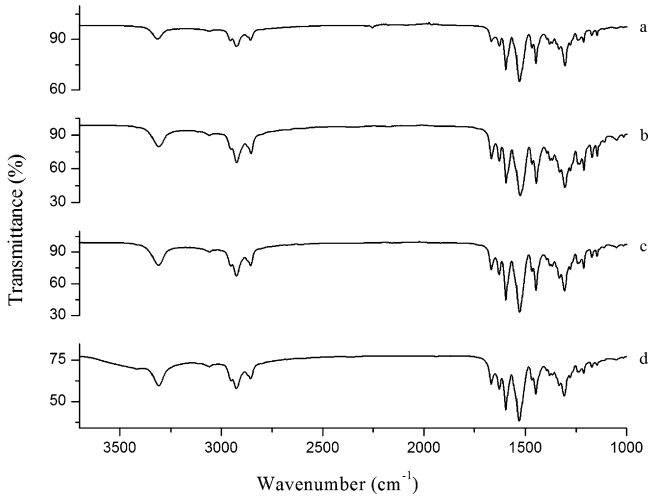

Fig. 5. FT-IR spectra of gelator **2** in (a) solution 12.0 mg/mL of $CDCl_3$, (b) 1 wt% of wet gel in cyclohexane, (c) 1 wt% of dried gel/xerogel in cyclohexane, and (d) solid powder.

A continuous red shift observed in short wavelength (SW) λ^{fl}_{max} with increase in polarity and hydrogen bonding nature of solvents indicates a greater charge transfer interaction from the substituents to naphthanilide ring and increase in the delocalization of lone pair of the hydroxy group and π cloud of the >C=O group throughout the aromatic ring in S_1 state (Fig. S11). On the other hand

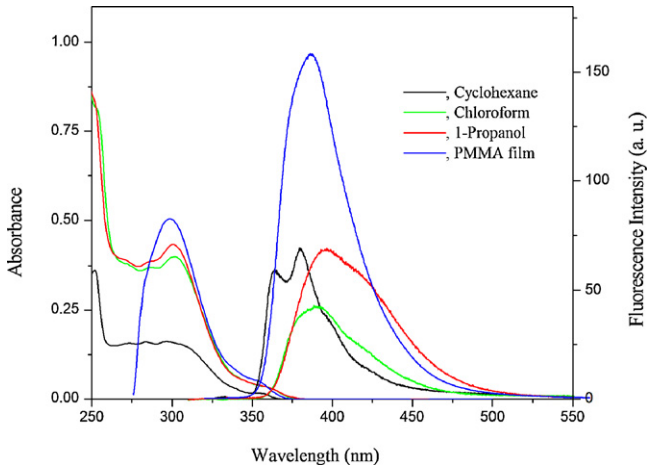

Fig. 6. UV–vis absorption at left and photoluminescence spectra at right of non-ESIPT chromophore **3** in selected solvents and a polymethylmethacrylate (PMMA) solid film.

under similar environments, LW λ^{fl}_{max} is blue shifted. Φ_{fl} of SW emission band increases and that of LW emission band decreases with increase in polarity and protic nature of the solvents. Whereas absorption band maxima for a long wavelength band centered on ~356 nm of compound **3** remain invariant. Only one small Stokes' shifted fluorescence band maxima (λ^{fl}_{max}) is red shifted under the same environments and Φ_{fl} first decreases from non-polar to polar aprotic then increases in polar protic solvents. Emission band is independent of excitation wavelength (λ_{exc}) in all the solvents, suggesting that emission is taking place from the most relaxed excited state in these solvents.

To examine the spectroscopic properties of self-assembled aggregates, UV–vis and photoluminescence spectra of gelator **2** were measured in solution (25 wt% of dioxane in cyclohexane), as well as in gels (cyclohexane/dodecane gels). Dioxane, which is miscible with cyclohexane, was used to disturb the intermolecular hydrogen bond. Three samples were prepared to compare the gel to the solution state, consisting of 0.5 wt% organogelator and 99.5 wt% dodecane/cyclohexane, and 25 wt% dioxane and 74.5 wt% cyclohexane and 0.5 wt% organogelator, respectively. In other words, the former is in gel state and the latter is in solution state. Fig. 2 shows the UV–vis and PL spectra for gelator **2** and Fig. 6 shows the UV and PL spectra for non-ESIPT analogue **3**. In the gels, *J*-aggregate formation resulted in a ~23–26 nm red shift of the UV–vis absorption band and the PL intensity from these gel states was ~30–32 fold increased relative to a solution of the same concentration. The fluorescence quantum yield (Φ_{PL}) of ESIPT gelator is 2.0×10^{-3}, 1.6×10^{-3}, 2.3×10^{-2}, 2.1×10^{-2} in cyclohexane, chloroform, methanol and PMMA film doped with 10 wt% of **2**, respectively. Whereas Φ_{PL} of non-ESIPT methoxy derivative is 5.4×10^{-2}, 1.5×10^{-2}, 2.1×10^{-2} and 1.2×10^{-1} in cyclohexane, chloroform, methanol and PMMA film doped with 10 wt% of **3**, respectively. The maximum emission peaks of both gels are located at 558 nm with a large Stokes' shift (180–182 nm) are observed relative to the absorption of the gels. This emission is thought to originate from the proton transferred keto (K*) form of molecule **2** (Figs. 1 and S10). Presence of enol emission suggests that the locally excited state decays (E*) mainly a competitive process rather effective ESIPT with only tautomer emission in both solution and gel state, which was further confirmed theoretically as summarized in Table 3. Enhanced fluorescence emission was observed not only from the gels, but also from solid state crystal and powder state of compounds **2** and **3**. These results suggest that the enhanced fluorescence emission of the gel is caused by the formation of molecular aggregations.

To further study the relationship between their molecular structures and optical properties, the geometrical parameters of keto–enol tautomers and their energy-minimized, preferred conformations were calculated by DFT using B3LYP/6-31G(d,p) and semi-empirical using AM1 calculations. The selected parameters

Table 3
Energetic characterization of keto form (K) and enol form (E) in ground (S_0) and excited (S_1) states in the gas phase.

AM1 (TDDFT)	S_0		S_1	
	HNAHPA-E	HNAHPA-K	HNAHPA-E	HNAHPA-K
E (kcal mol^{-1})	0 (0)	12.1 (16.39)	13.4 (37.81)	0 (0)
μ (D)	3.92 (6.34)	8.41 (9.56)	2.55	6.73
φ_1 (°)	36.7 (9.4)	16.9 (0.6)	33.1	24.6
φ_2 (°)	178.6 (176.4)	166.5 (179.6)	179.5	166.0
φ_3 (°)	161.5 (168.6)	160.4 (166.4)	162.3	162.7
φ_4 (°)	46.1 (26.1)	42.8 (25.9)	45.6	40.0
Excitation energy (nm)	311 (385)	508 (542)		
Emission energy (nm)	336	706		

are summarized along with experimentally observed absorption and emission maxima in Table 3. Dihedral angles (φ), and dipole moments (μ) in both S_0 and S_1 states of keto–enol tautomeric forms of compound **2** clearly display a planar naphthanilide with twisted alkyl amide side chain (Figs. S10 and S11).

It must be noted that the geometry of the keto form in the ground state (S_0) was optimized, keeping the O_a–H distance, the same as that of O_d–H distance in the optimized geometry of enol form. Otherwise, optimization will reverse back to the enol form here, O_d and O_a refer to the donor and acceptor oxygen atoms in the enol form, respectively. The results of the calculations demonstrate that the enol form is most stable and the keto form is 16.39 kcal mol^{-1} higher in energy. But, in the first excited singlet state (S_1) the keto form is 37.81 kcal mol^{-1} more stable than the enol form. Results of AM1 calculations also predict similar results, except that the enol form is 12.1 kcal mol^{-1} more stable than the keto form in S_0 state, whereas the keto form is 13.4 kcal mol^{-1} more stable than the corresponding enol form in S_1 state under isolated conditions. The transformation from enol to keto in the S_0 and S_1 states can be thought of as arising from proton transfer from O_d to O_a, with concomitant redistribution of electron density in and around the six-membered hydrogen bonded ring. Alternatively, one could view this as a hydrogen atom transfer. In either case, one needs to identify the 'reaction co-ordinate' and investigate the potential energy change along the reaction coordinate. As the proton translocation distance of the mobile hydrogen atom is considered to be a key parameter for the construction of the ESIPT potential, the O_d–H distance $r_{(O_d-H)}$ was varied between what is normal for the primary and what is known to be the equilibrium tautomeric O_d–H distance. At each such point, all other geometrical parameters were fully optimized (with 8-configuration CI in S_0 and S_1 states), and the total energy (ΔE_t) was plotted against $r_{(O_d-H)}$ using the AM1 method (Fig. 7). The resulting potential energy (PE) profile again reveals that the enol form is most stable in the ground state whereas the keto form is most stable in the first excited singlet (S_1) state. The barrier for the enol to keto transformation is substantial: 22.37 kcal mol^{-1}, large enough to make ground state intramolecular proton transfer (GSIPT) unviable (E → K) under thermal conditions, whereas upon photoexcitation, much smaller interconversion barrier (E* → K*) of 4.39 kcal mol^{-1} in S_1 state preferably allows ESIPT to give the large Stokes' shifted tautomer emission (9245 cm^{-1}). After decaying to the ground state, the keto form reverts to the original enol form via reverse proton transfer barrier (K → E) of 8.83 kcal mol^{-1}. Moreover, the intrinsic four-level process (E → E* → K* → K → E) provides an ideal scheme for stimulated emission by easy population inversion of the proton transferred keto form.

It is worth to be mentioned here that naphthanilide gelator **2** gives dual emission (orange color) in cyclohexane solution and solid film state at 446, 574 and 393, 558 nm and quantum efficiency 0.002 and 0.021, whereas under similar condition its resemblance *N*-heptyl-2-(2-hydroxybenzamido)benzamide (salicylanilide gelator) [Ref. 36] gives only tautomer emission (blue color) in cyclohexane solution and solid film state at 472 and 465 nm and quantum efficiency 0.108 and 0.182, respectively. However, the potential energy profile for enol to keto and reverse proton transfer from keto to enol transformations upon photoexcitation reveals that the barriers of 4.39 and 8.83 kcal mol^{-1} for naphthanilide gelator **2** whereas, these barriers are reduced to 2.39 and 5.67 kcal mol^{-1} for salicylanilide gelator [36]. Smaller interconversion barrier (E* → K*) of 2.39 kcal mol^{-1} in S_1 state of salicylanilide gelator allows highly efficient ESIPT to give only the large Stokes' shifted tautomer emission (9773 cm^{-1}) whereas, higher interconversion barrier (E* → K*) of 4.39 kcal mol^{-1} in S_1 state of gelator **2** moreover allows competing processes originating from both locally excited (normal emission) and tautomer emission (9245 cm^{-1}) as a result of dual emission. Interestingly, the fluorescence enhancement accompanying gelation **2** is ~4 folds higher than salicylanilide gelation induced enhancement.

Apart from the above mentioned chromophores, there are several others that have been developed and reported recently samples with enhanced emission induced by molecular aggregation [34–38] and suggested that the enhanced fluorescence can be explained by the planar conformation in the solid state, which can activate the radiation process [39,40]. In the solution state, the molecule remains twisted to some extent due to steric interactions, which suppress the radiation process. On the other hand, in the gel state aggregation induced planarization due to strong intermolecular hydrogen bonding extends the effective π-conjugation which activates the radiation process. These intermolecular hydrogen bonds probably reduce the bond rotation within gelator molecule that prevents the nonradiative transition and as a result of that fluorescence enhancement also occurs to some extent [41]. The absorption

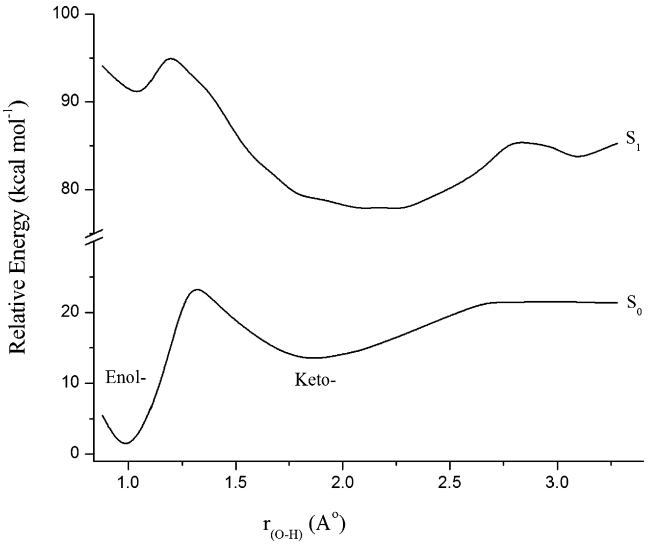

Fig. 7. Potential energy profile for intramolecular proton transfer in the ground and excited states of **2** obtained by varying $r_{(O_d-H)}$ and optimize the rest of structural parameters for each choice of $r_{(O_d-H)}$ using AM1/PECI = 8 calculation.

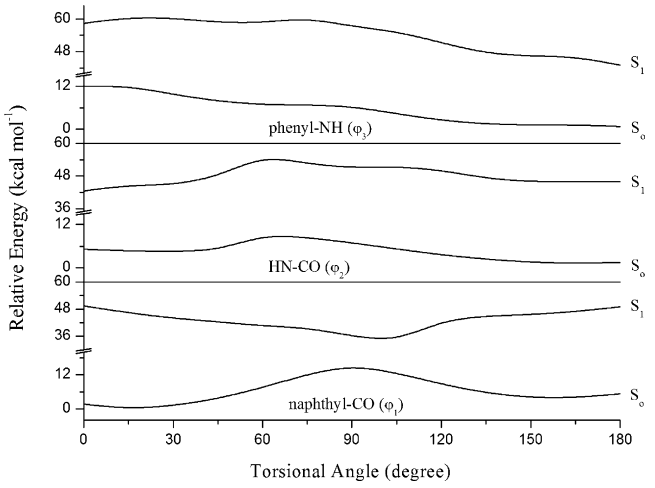

Fig. 8. Potential energy profiles for the keto forms of compound **2** in the ground (K) and excited (K*) singlet states with respect to the torsional angle around the naphthyl–CO, HN–CO, and phenyl–NH bond rotations using AM1/PECI = 8 calculation.

band of the gel with a red-shift of ~23–26 nm relative to that in solution, also contributes towards the molecular planarization to the enhanced emission. It is well known that an increase in the rigidity of a molecule can decrease molecular vibrations, probably suppress the internal conversion (IC) or twisted intra-molecular charge transfer (TICT) of an excited molecule, and may increase the fluorescence quantum yield [38,42]. In addition, the fluorescence intensity of the π-conjugated chromophores is correlated with the π aggregation, such as *H* and *J* aggregations [40]. *H* aggregations, in which the molecules are aligned in parallel to each other in a head-to-head form, tend to increase the internal conversion from a higher electronic state into a lower one so that the fluorescence emission is effectively quenched. In contrast, the molecules are arranged into a head-to-tail stack as in *J* aggregation, in which the transition from the lower couple excited state of the molecule to the ground state is allowed; as a result, the absorption peak will red-shift and the fluorescence emission will be stronger than that of the monomer [43]. In our case, the gelator molecules form *J* aggregations and cross-link into a solid-like 3D network in the gel phase, so the enhanced emission of the gel is attributed to the synergetic effect of the restricted molecular motion and the formation of *J* aggregations.

In Fig. 8, the geometry dependent potential energies in the S_0 and S_1 states for the keto forms of ESIPT gelator **2** are displayed. The rotations around the three flexible bonds have been analyzed that can change their conformations in excited states; two aromatic amide bonds (naphthyl–CO, φ_1 and phenyl–NH, φ_3) and the amide bond itself (HN–CO, φ_2) by changing geometrical parameters of interest from the optimized geometry of **2**. For the aromatic amide bond (naphthyl–CO) twist in the excited state, the potential curve shows the maximum values at 0° and the minimum at 105°. The appearance of S_1 potential energy surface indicates that there is no barrier for large amplitude twisting about the naphthyl–CO bond. Furthermore, the maximum at 90° in the S_0 state produces a smaller gap between the ground and first excited states. As a result, the non-radiative transition from the minimum in S_1 to the ground state is likely to be important; consequently, this structure can be expected to lead to the quenching of the keto fluorescence. As for the rotation around the amide bond (HN–CO) in the S_1 state, potential energy curve shows a maximum at 60° thereby producing an estimated activation barrier of 11.44 kcal mol^{-1}. In the potential energy profile for the rotation around phenyl–NH in the excited state, we have found only one maximum at 75° with an interconversion barrier of 16.12 kcal mol^{-1}. Gelation-induced fluorescence emission observed in **2** could then be rationalized and supported by combining these theoretical calculations with the previously suggested molecular orbital (MO) calculations on deactivation processes of the *N*-salicylideneanils [44], and *ortho*-substituted *N*-heptyl amide of salicylanilides [36], the most probable rotation involving the keto-rotated species is the phenyl–CO bond. Under such conditions, the fluorescence of the *cis*-keto* isomer can be quenched by dynamic internal torsion processes in the excited state leading to the formation of *twisted*-keto* (Fig. 1). This species, accessed after ESIPT, involves a twisted intramolecular charge transfer state (TICT), which brings about the fluorescence quenching observed in solution. Accordingly, the fluorescence enhancement in the solid state is due to the prevented TICT by kinetic constraint which blocks large amplitude twisting motion. In essence, the enhanced fluorescent behavior of gelators was attributed to its rigid structure, which precludes extensive twisting about the naphthyl–CO bond (torsion angle, φ_1) along the ESIPT reaction coordinate. This allowed the tuning of emission by controlling the degree of aggregation, which might be useful in the design of fluorescent labels [45] and optical sensors [46].

4. Conclusion

Highly emissive organogelator **2** containing ESIPT moiety bearing a chelating platform was synthesized and characterized. Through combining the results of FT-IR, UV–vis absorption, photoluminescence and DFT, semi-empirical (AM1) calculations, the molecular packing model in the gel phase was deduced. It has been demonstrated that gelator **2** is self-assembled into complex 3-D networks and their aggregation into fibrous superstructures is driven by π–π stacking interactions between the central naphthanilide moieties, hydrogen-bonding interactions among the amide, OH···O=C groups, and van der Waals interactions among the alkyl groups. In the gels, *J*-aggregate formation resulted in a ~23–26 nm red shift of the UV–vis absorption band and the PL intensity from these gel states was ~30–32 folds higher than that of the solution phase. It was found that the nonradiative relaxation process via TICT is reduced in the hydrogen bonded supramolecular assembly and gel states leading to the enhanced ESIPT emission.

Acknowledgments

The author is gratefully acknowledged to Professor Soo Young Park, Department of Materials Science and Engineering, Seoul National University, Seoul, South Korea, for useful discussions and comments. I would also like to be grateful to Professor Hassan S. Bazzi, Department of Chemistry, Texas A&M University at Qatar, Doha, Qatar for giving me technical knowledge in several fields.

Appendix A. Supplementary data

Supplementary data associated with this article can be found, in the online version, at doi:10.1016/j.jphotochem.2010.09.014.

References

[1] (a) P. Terech, R.G. Weiss, Chem. Rev. 97 (1997) 3133–3159;
(b) J.H. van Esch, B.L. Feringa, Angew. Chem. Int. Ed. 39 (2000) 2263–2266;
(c) L.A. Estorff, A.D. Hamilton, Chem. Rev. 104 (2004) 1201–1217;
(d) T. Ishi-I, S. Shinkai, Top. Curr. Chem. 258 (2005) 119–160;
(e) F. Camerel, L. Bonardi, M. Schmutz, R. Ziessel, J. Am. Chem. Soc. 128 (2006) 4548–4549;
(f) A. Brizard, R. Oda, I. Huc, Top. Curr. Chem. 256 (2005) 167–218.
[2] (a) A. Ajayaghosh, V.K. Praveen, Acc. Chem. Res. 40 (2007) 644–656;
(b) C. Wang, D. Zhang, D. Zhu, Langmuir 23 (2007) 1478–1482.
[3] (a) S. Das, S. Varghese, N.S.S. Kumar, Langmuir 26 (2010) 1598–1609;
(b) C. Wang, Q. Chen, F. Sun, D. Zhang, G. Zhang, Y. Huang, R. Zhao, D. Zhu, J. Am. Chem. Soc. 132 (2010) 3092–3096.

[4] H. Komatsu, S. Matsumoto, S.-I. Tamaru, K. Kaneko, M. Ikeda, I. Hamachi, J. Am. Chem. Soc. 131 (2009) 5580–5585.
[5] (a) X. Chen, Z. Huang, S.-Y. Chen, K. Li, X.-Q. Yu, L. Pu, J. Am. Chem. Soc. 132 (2010) 7297–7299;
(b) M.-O.M. Piepenbrock, G.O. Lloyd, N. Clarke, J.W. Steed, Chem. Rev. 110 (2010) 1960–2004;
(c) F. Fages, Angew. Chem. Int. Ed. 45 (2006) 1680–1682.
[6] (a) A.R. Hirst, B. Escuder, J.F. Miravet, D.K. Smith, Angew. Chem. Int. Ed. 47 (2008) 8002–8018;
(b) N.M. Sangeetha, U. Maitra, Chem. Soc. Rev. 34 (2005) 821–836.
[7] (a) H. Dai, Q. Chen, H. Qin, Y. Guan, D. Shen, Y. Hua, Y. Tang, J. Xu, Macromolecules 39 (2006) 6584–6589;
(b) R.M.K. Ramanan, P. Chellamuthu, L. Tang, K.T. Nguyen, Biotechnol. Prog. 22 (2006) 118–125.
[8] (a) J.W. Chung, B.-K. An, S.Y. Park, Chem. Mater. 20 (2008) 6750–6755;
(b) X. Tong, Y. Zhao, B.-K. An, S.Y. Park, Adv. Funct. Mater. 16 (2006) 1799–1804;
(c) A. Kishimura, T. Yamashita, T. Aida, J. Am. Chem. Soc. 127 (2005) 179–183.
[9] (a) M. Carrasco-Orozco, W.C. Tsoi, M. O'Neill, M.P. Aldred, P. Vlachos, S.M. Kelly, Adv. Mater. 18 (2006) 1754–1758;
(b) F. Camerel, R. Ziessel, B. Donnio, C. Bourgogne, D. Guillon, M. Schmutz, C. Iacovita, J.-P. Bucher, Angew. Chem. Int. Ed. 46 (2007) 2659–2662.
[10] (a) H. Yang, T. Yi, Z. Zhou, Y. Zhou, J. Wu, M. Xu, F. Li, C. Huang, Langmuir 23 (2007) 8224–8230;
(b) Q. Liu, Y. Wang, W. Li, L. Wu, Langmuir 23 (2007) 8217–8223;
(c) T.H. Kim, D.G. Kim, M. Lee, T.S. Lee, Tetrahedron 66 (2010) 1667–1672;
(d) P. Mukhopadhyay, Y. Iwashita, M. Shirakawa, S.-I. Kawano, N. Fujita, S. Shinkai, Angew. Chem. Int. Ed. 45 (2006) 1592–1595;
(e) A. Ghoussoub, J.-M. Lehn, Chem. Commun. (2005) 5763–5765;
(f) Z. Dzolic, A.D. Cametti, A.D. Cort, L. Mandolini, M. Zinic, Chem. Commun. (2007) 3535–3537.
[11] (a) S. Wang, W. Shen, Y. Feng, H. Tian, Chem. Commun. (2006) 1497–1499;
(b) M. Shirakawa, N. Fujita, T. Tani, K. Kaneko, M. Ojima, A. Fujii, M. Ozaki, S. Shinkai, Chem. Eur. J. 13 (2007) 4155–4162;
(c) K. Sugiyasu, N. Fujita, S. Shinkai, J. Mater. Chem. 15 (2005) 2747–2754;
(d) J. Puigmartí-Luis, V. Laukhin, Á. Pérez del Pino, J. Vidal-Gancedo, C. Rovira, E. Laukhina, D.B. Amabilino, Angew. Chem. Int. Ed. 46 (2007) 238–241;
(e) L. Schmidt-Mende, A. Fechtenkotter, E. Moons, R.H. Friend, J.D. Mack-Enzie, Science 293 (2001) 1119–1122;
(f) Z. Huo, S. Dai, C. Zhang, F. Kong, X. Fang, L. Guo, W. Liu, L. Hu, X. Pan, K. Wang, J. Phys. Chem. B 112 (2008) 12927–12933;
(g) K. Sugiyasu, S.-i. Kawano, N. Fujita, S. Shinkai, Chem. Mater. 20 (2008) 2863–2865.
[12] (a) V.K. Praveen, S.J. George, R. Varghese, C. Vijayakumar, A. Ajayaghosh, J. Am. Chem. Soc. 128 (2006) 7542–7550;
(b) J.H. Jung, S.J. Lee, J.A. Rim, H. Lee, T.-S. Bae, S.S. Lee, S. Shinkai, Chem. Mater. 17 (2005) 459–462.
[13] (a) A. Ajayghosh, V.K. Praveen, C. Vijayakumar, Chem. Soc. Rev. 37 (2008) 109–122;
(b) K. Sugiyasu, N. Fujita, S. Shinkai, Angew. Chem. Int. Ed. 43 (2004) 1229–1233;
(c) T. Nakashima, N. Kimizuka, Adv. Mater. 14 (2004) 1113–1116.
[14] X. Zhang, L. Guo, F.-Y. Wu, Y.-B. Jiang, Org. Lett. 5 (2003) 2667–2670.
[15] H. Mishra, J. Phys. Chem. B 110 (2006) 9387–9396.
[16] L. Zhao, C. YaoHan, J. YunBao, Sci. China Ser. B: Chem. 52 (2009) 786–792.
[17] (a) S.K. Dubey, A.K. Singh, H. Singh, S. Sharma, R.N. Iyer, J.C. Katiyar, P. Goel, A.B. Sen, J. Med. Chem. 21 (1978) 1178–1181;
(b) H. Singh, S. Sharma, R.N. Iyer, J.C. Katiyar, A.B. Sen, Z. Naturforsch. C 33 (1978) 447–448.
[18] K.C. Tsou, S. Matsukawa, J. Med. Chem. 11 (1968) 1097–1099.
[19] M.K. Nayak, J. Seo, S. Park, S.Y. Park, J. Photochem. Photobiol. A: Chem. 191 (2007) 228–232.
[20] I.B. Berlman, Handbook of Fluorescence Spectra of Aromatic Molecules, Academic Press, New York, 1971.
[21] J.C. de Mello, H.F. Wittmann, R.H. Friend, Adv. Mater. 9 (1997) 230–232.
[22] A.D. Becke, J. Chem. Phys. 98 (1993) 5648–5652.
[23] J. Llano, J. Raber, L.A. Eriksson, J. Photochem. Photobiol. A: Chem. 154 (2003) 235–243.
[24] (a) R. Bauernschmitt, R. Ahlrichs, F.H. Hennrich, M.M. Kappes, J. Am. Chem. Soc. 120 (1998) 5052–5059;
(b) M.E. Casida, J. Chem. Phys. 108 (1998) 4439–4449;
(c) R.E. Stratmann, G.E. Scuseria, M.J. Frisch, J. Chem. Phys. 109 (1998) 8218–8224.
[25] J. Llano, L.A. Eriksson, Phys. Chem. Chem. Phys. 6 (2004) 4707–4713.
[26] M.J. Frisch, G.W. Trucks, H.B. Schlegel, G.E. Scuseria, M.A. Robb, J.R. Cheeseman, J.A. Montgomery, T. Vreven, K.N. Kudin, J.C. Burant, J.M. Millam, S.S. Iyengar, J. Tomasi, V. Barone, B. Mennucci, M. Cossi, G. Scalmani, N. Rega, G.A. Petersson, H. Nakatsuji, M. Hada, M. Ehara, K. Toyota, R. Fukuda, J. Hasegawa, M. Ishida, T. Nakajima, Y. Honda, O. Kitao, H. Nakai, M. Klene, X. Li, J.E. Knox, H.P. Hratchian, J.B. Cross, C. Adamo, J. Jaramillo, R. Gomperts, R.E. Stratmann, O. Yazyev, A.J. Austin, R. Cammi, C. Pomelli, J.W. Ochterski, P.Y. Ayala, K. Morokuma, G.A. Voth, P. Salvador, J.J. Dannenberg, V.G. Zakrzewski, S. Dapprich, A.D. Daniels, M.C. Strain, O. Farkas, D.K. Malick, A.D. Rabuck, K. Raghavachari, J.B. Foresman, J.V. Ortiz, Q. Cui, A.G. Baboul, S. Clifford, J. Cioslowski, B.B. Stefanov, G. Liu, A. Liashenko, P. Piskorz, I. Komaromi, R.L. Martin, D.J. Fox, T. Keith, M.A. Al-Laham, C.Y. Peng, A. Nanayakkara, M. Challacombe, P.M.W. Gill, B. Johnson, W. Chen, M.W. Wong, C. Gonzalez, J.A. Pople, Gaussian 03, revision B.03, Gaussian Inc., Pittsburgh, PA, 2003.
[27] (a) M.J.S. Dewar, E.G. Zoebisch, E.F. Healy, J.J.P. Stewart, J. Am. Chem. Soc. 107 (1985) 3902–3909;
(b) G.B. Rocha, R.O. Freire, A.M. Simas, J.J.P. Stewart, J. Comput. Chem. 27 (2006) 1101–1111.
[28] G. Rauhut, T. Clark, T. Steinke, J. Am. Chem. Soc. 115 (1993) 9174–9181.
[29] (a) H. Mishra, S. Maheshwary, H.B. Tripathi, N. Sathyamurthy, J. Phys. Chem. A 109 (2005) 2746–2754;
(b) R. Misra, A. Mandal, M. Mukhopadhyay, D.K. Maity, S.P. Bhattacharyya, J. Phys. Chem. B 113 (2009) 10779–10791;
(c) S. Mitra, R. Das, S.P. Bhattacharyya, S. Mukherjee, J. Phys. Chem. A 101 (1997) 293–298.
[30] M.K. Nayak, S.K. Dogra, J. Photochem. Photobiol. A: Chem. 169 (2005) 79–88;
M.K. Nayak, S.K. Dogra, J. Photochem. Photobiol. A: Chem. 161 (2004) 169–183;
M.K. Nayak, S.K. Dogra, Spectrochim. Acta A 61 (2005) 1247–1257.
[31] J.D. Jong, J.D.L.N.R. Lucas, M. Kellog, J.H. van Esch, B.L. Feringa, Science 304 (2004) 278–281.
[32] (a) S.K. Samanta, A. Pal, S. Bhattacharya, Langmuir 25 (2009) 8567–8578;
(b) H. Basit, A. Pal, S. Sen, S. Bhattacharya, Chem. Eur. J. 14 (2008) 6534–6545;
(c) A. Pal, Y.K. Ghosh, S. Bhattacharya, Tetrahedron 63 (2007) 7334–7348.
[33] T. Kar, S. Debnath, D. Das, A. Shome, P.K. Das, Langmuir 25 (2009) 8639–8648.
[34] G. Palui, A. Banerjee, J. Phys. Chem. B 112 (2008) 10107–10115.
[35] (a) J. Peng, K. Liu, X. Liu, H. Xia, J. Liu, Y. Fang, New J. Chem. 32 (2008) 2218–2224;
(b) M. Teng, G. Kuang, X. Jia, M. Gao, Y. Li, Y. Wei, J. Mater. Chem. 19 (2009) 5648–5654.
[36] M.K. Nayak, B.-H. Kim, J.E. Kwon, S. Park, J. Seo, J.W. Chung, S.Y. Park, Chem. Eur. J. 16 (2010) 7437–7447.
[37] (a) J. Seo, J.W. Chung, E.-H. Jo, S.Y. Park, Chem. Commun. (2008) 2794–2796;
(b) J. Luo, Z. Xie, J.W.Y. Lam, L. Cheng, H. Chen, C. Qiu, H.S. Kwok, X. Zhan, Y. Liu, D. Zhu, B. Tang, Chem. Commun. (2001) 1740–1741.
[38] (a) P. Chen, R. Lu, P. Xue, T. Xu, G. Chen, Y. Zhao, Langmuir 25 (2009) 8395–8399;
(b) P. Xue, R. Lu, G. Chen, Y. Zhang, H. Nomoto, M. Takafuji, H. Ihara, Chem. Eur. J. 13 (2007) 8231–8239.
[39] (a) Y. Chen, Y. Lv, Y. Han, B. Zhu, F. Zhang, Z. Bo, C.-Y. Liu, Langmuir 25 (2009) 8548–8555;
(b) S. Kim, Q. Zheng, G.S. He, D.J. Bharali, H.E. Pudavar, A. Baev, P.N. Prasad, Adv. Funct. Mater. 16 (2006) 2317–2323.
[40] (a) S. Abraham, R.K. Vijayaraghavan, S. Das, Langmuir 25 (2009) 8507–8513;
(b) B. An, S. Kwon, S. Jung, S.Y. Park, J. Am. Chem. Soc. 124 (2002) 14410–14415.
[41] C. Wang, D. Zhang, J. Xiang, D. Zhu, Langmuir 23 (2007) 9195–9200.
[42] (a) C.Y. Bao, R. Lu, M. Jin, P.C. Xue, C.H. Tan, G.F. Liu, Y.Y. Zhao, Org. Biomol. Chem. 3 (2005) 2508–2512;
(b) S. Bhattacharya, S.K. Samanta, Langmuir 25 (2009) 8378–8381;
(c) F.D. Lewis, W. Liu, J. Phys. Chem. A 106 (2002) 1976–1984.
[43] (a) S. Varghese, N.S.S. Kumar, A. Krishna, D.S.S. Rao, S.K. Prasad, S. Das, Adv. Funct. Mater. 19 (2009) 2064–2073;
(b) A. Chowdhury, S. Wachsmann-Hogiu, P.R. Bangal, I. Raheem, L.A. Peteanu, J. Phys. Chem. B 105 (2001) 12196–12201.
[44] (a) V.C. Vargas, J. Phys. Chem. A 108 (2004) 281–288;
(b) F. Robert, A.D. Naik, B. Tinant, R. Robiette, Y. Garcia, Chem. Eur. J. 15 (2009) 4327–4342.
[45] F. Camerel, L. Bonardi, G. Ulrich, L. Charbonniere, B. Donnio, C. Bourgogne, D. Guillon, P. Retailleau, R. Ziessel, Chem. Mater. 18 (2006) 5009–5021.
[46] A.N. Shipway, E. Katz, I. Willner, ChemPhysChem 1 (2000) 18–52.